Notes on Neff et al. (2023) AMOC Box Model Study

Jicheng Duan[a], [1]

[a]School of Mathematics and Physics, China University of Geosciences, Wuhan, China

Abstract

This note reviews the three-box model for AMOC used in Neff et al. (Physica D, 2023, 456: 133907), focusing on both the symmetric and asymmetric cases. It summarizes the model equations, key bifurcation results, and outlines the numerical method used to identify multiple equilibria. Notably, under certain parameter settings, the system exhibits up to four coexisting stable equilibria. To explore rate-induced tipping, a non-autonomous extension is proposed by introducing a timedependent freshwater forcing $F(t) = F_0 + rt$, motivated by gradual climate processes such as ice melt. To better understand the dynamical mechanisms behind R-tipping, a simpler bistable driveresponse system is also studied. This example shares a similar phase space structure with the threebox model and illustrates how tipping can occur due to drift speed alone. I would like to discuss whether rate-induced tipping is worth exploring in the three-box model, and whether the presence of non-smooth bifurcations and absolute value terms could lead to qualitatively new dynamical features.

1. Three-box model

Let me first briefly review the structure of the model used in this paper, as well as some key results and numerical implementations from the bifurcation analysis presented in Section 3 of the study by Neff et al., titled "Bifurcation analysis of a North Atlantic Ocean box model with two deep-water formation sites", published in Physica D (2023) 456: 133907.

1.1. Model 1

To investigate the stability and transitions of the Atlantic Meridional Overturning Circulation (AMOC), the authors construct a low-dimensional dynamical system consisting of three connected ocean boxes. These represent the Labrador Sea (box L), the Nordic Seas (box N), and the midlatitude Atlantic (box A). While surface temperatures T_L, T_N, and T_A are assumed to be fixed, salinities S_L, S_N, and S_A evolve dynamically and play a central role in determining water density and hence the circulation strength.

[1]corresponding author. E-mail address: jichengduan9708@163.com

The governing equations for the salinities in the polar boxes L and N are derived from salt conservation and take the form:

$$V_L \frac{dS_L}{dt} = -\left(F + F_L\right) S_0 + |q_L| \left(S_A - S_L\right),$$
$$V_N \frac{dS_N}{dt} = -\left(F + F_N\right) S_0 + |q_N| \left(S_A - S_N\right),$$

where F is the external freshwater forcing applied uniformly, while F_L and F_N represent background freshwater fluxes into boxes L and N, respectively. S_0 denotes a reference salinity, and V_L, V_N, and V_A are the volumes of the respective boxes. The salinity in the mid-latitude box A, denoted S_A, is not dynamically evolved but computed at each time from the global salt conservation constraint:

$$V_L S_L + V_A S_A + V_N S_N = V_{\text{tot}} S_0,$$

where $V_{\text{tot}} = V_L + V_A + V_N$ is the total ocean volume. The advective flow strengths q_L and q_N are driven by the density differences between each polar box and the mid-latitude box. Assuming linear dependence of density on temperature and salinity, the flows are given by:

$$q_L = -k \left[\alpha \left(T_L - T_A\right) - \beta \left(S_L - S_A\right)\right],$$
$$q_N = -k \left[\alpha \left(T_N - T_A\right) - \beta \left(S_N - S_A\right)\right],$$

where α and β are the thermal expansion and haline contraction coefficients, respectively, and k is a hydraulic constant. Positive values of q_L and q_N correspond to downwelling (i.e., deep-water formation) in the respective polar regions.

In the symmetric version of the model, referred to as Model 1, the freshwater and thermal forcings into boxes L and N are identical. That is, $F_L = F_N$ and $T_L = T_N$. Under this assumption, the model possesses symmetry under the exchange $S_L \leftrightarrow S_N$, and the bifurcation structure is correspondingly constrained. As the control parameter F is varied, the model exhibits multiple equilibria, including a strong overturning state (pattern I), a collapsed state with no downwelling (pattern II), and two asymmetric intermediate states (patterns III and IV) in which only one of the two polar regions sustains deep convection. However, in the symmetric model, these intermediate states are dynamically inaccessible under generic parameter sweeps, as they lie on solution branches that are not connected through bifurcations encountered during typical freshwater hosing experiments.

1.2. Model 2

To reflect the asymmetric nature of real-world AMOC, the authors introduce a generalized model, Model 2, in which asymmetries in freshwater and thermal forcing between the two polar boxes are parameterized by two quantities, η and μ. The freshwater flux into box L is interpolated as:

$$F_L = F_N + \eta \left(F_L^{\text{nom}} - F_N\right),$$

where F_N is the reference value (symmetric case), and F_L^{nom} is the observed nominal value. Similarly, the temperature of box L is set by:

$$T_L = T_N + \mu \left(T_L^{\text{nom}} - T_N\right),$$

where T_N is the fixed Nordic temperature and T_L^{nom} is the observed Labrador Sea surface temperature. The complete system is thus:

$$\begin{aligned}
\frac{dS_L}{dt} &= -\frac{1}{V_L}\left(F(t) + F_N + \eta\left(F_L - F_N\right)\right) S_0 + \frac{1}{V_L}\left|q_L\right|\left(S_A - S_L\right), \\
\frac{dS_N}{dt} &= -\frac{1}{V_N}\left(F(t) + F_N\right) S_0 + \frac{1}{V_N}\left|q_N\right|\left(S_A - S_N\right), \\
S_A &= \frac{V_{\text{tot}} S_0 - V_L S_L - V_N S_N}{V_A}, \\
q_L &= -k\left[\alpha\left(T_N + \mu\left(T_L - T_N\right) - T_A\right) - \beta\left(S_L - S_A\right)\right], \\
q_N &= -k\left[\alpha\left(T_N - T_A\right) - \beta\left(S_N - S_A\right)\right].
\end{aligned}$$

When $\eta = \mu = 0$, the model reduces to the symmetric configuration (Model 1). When $\eta = \mu = 1$, it reflects full observational asymmetry.

These asymmetries have profound consequences for the bifurcation structure. The introduction of asymmetry breaks the degeneracy of the fold bifurcations: instead of a simultaneous collapse of multiple equilibrium branches, the model exhibits distinct bifurcation points associated with different collapse paths. Notably, pattern IV, in which only the Nordic Seas remain active, becomes a dynamically accessible intermediate state. As freshwater forcing increases, the system may follow a multi-stage tipping path, transitioning from pattern I (both L and N active), through pattern IV (only N active), to pattern II (no deep-water formation). A reverse path may be followed during recovery. Additionally, the type of asymmetry plays a distinct role in the bifurcation behavior. Freshwater asymmetry, controlled by η, primarily affects the fold bifurcations at lower values of F, shifting the location where the lower branch (pattern II) terminates. In contrast, thermal asymmetry, governed by μ, more strongly influences the upper branch. In particular, it destabilizes the strong circulation state at a lower F value and causes pattern III (only L active) to exist as an isolated branch (isola), which cannot be accessed without carefully tuned initial conditions.

This is a reproduction of Figs. 9 and 10 from Section 3, along with an outline of the corresponding numerical algorithm. Please note that the model 1 implemented corresponds to the more general version, namely model 2, as described earlier. To recover the symmetric case, it is sufficient to set $\eta = 0$ and $\mu = 0$.

Algorithm 1: Multi-Equilibria Detection in Generalized Three-Box AMOC Model

Input: Physical parameters (Table 1); asymmetry controls η, μ;
Forcing range $F \in [F_{\min}, F_{\max}]$; number of steps N_F;
Initial salinity grid over (S_L, S_N); solver tolerance tol
Output: Equilibria (S_L, S_N, Q) and stability flags over all F

1. Discretize F into N_F points: F_i
2. Generate N_G diverse initial guesses for (S_L, S_N) over physical range
3. **for** $i = 1$ to N_F **do** // scan across F
4. **for** $j = 1$ to N_G **do** // loop over initial guesses
5. Solve $\dot{S}_L = \dot{S}_N = 0$ using `fsolve`
6. Discard duplicates (within 10^{-3} tolerance) or unphysical salinities
7. Linearize system at solution, compute Jacobian J
8. Set `stability = 1` if all eigenvalues of J have negative real part, else -1
9. Compute S_A from salt conservation
10. Calculate total overturning $Q = q_L + q_N$
11. Store $(F_i, S_L, S_N, Q, \texttt{stability})$
12. **end for**
13. **end for**
14. Plot bifurcation diagrams: (F, S_N), (F, S_L) and (F, Q) colored by stability

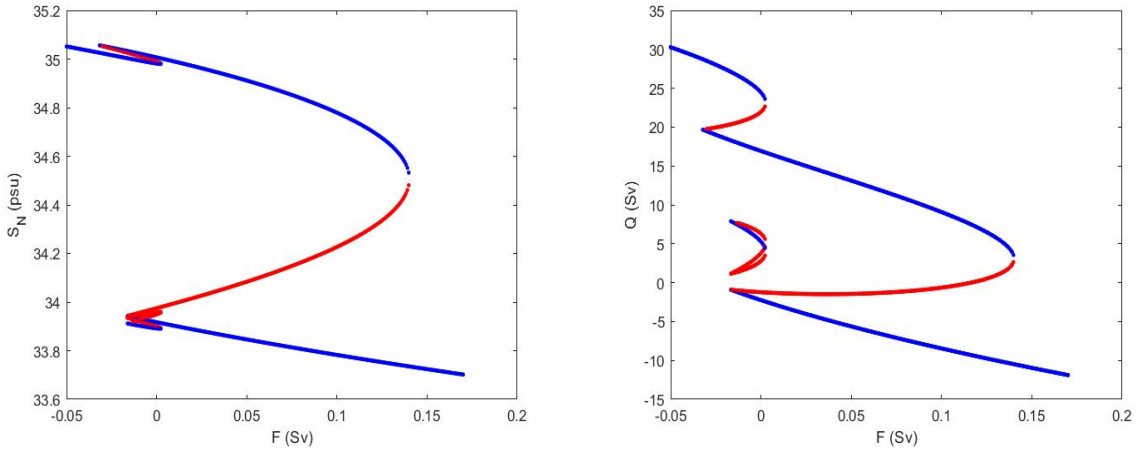

(a) (b)

Figure 1: Bifurcation diagram for the asymmetric case $(\eta, \mu) = (1, 1)$. The control parameter is the freshwater forcing F. Blue curves indicate branches of stable equilibria, while red curves denote unstable or saddle-type equilibria. Panels display the evolution of salinities S_N and total overturning strength Q as F varies.

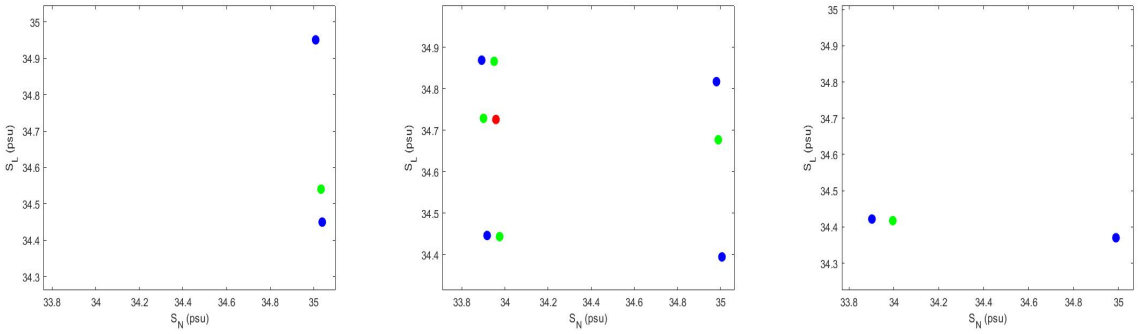

(a) (b) (c)

Figure 2: Phase plane diagrams for the asymmetric case $(\eta, \mu) = (1, 1)$ at three different freshwater forcing values: $F = -0.02$ (a), $F = 0$ (b), and $F = 0.01$ (c). Blue dots indicate stable equilibria, green dots denote saddle points, and red dots represent unstable equilibria.

It is important to note that this system, whether in the symmetric or asymmetric configuration, exhibits multistability under certain parameter conditions. In particular, there can be up to four coexisting stable equilibria, which is a key feature worth highlighting. I will illustrate this later with an example, as it plays a significant role in my own research.

2. Tipping poingts

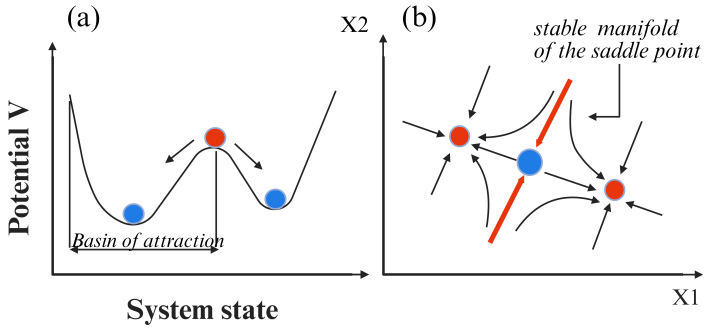

Figure 3

In many cases, tipping phenomena require the simultaneous existence of several different stable states of a system under the same given environmental conditions. Bistability and multistability can best be illustrated by a stability landscape represented as a potential, see Fig. 3(a). The stable states are in the valleys, while the unstable states are on the hills. Here, stability of a state means linear stability with respect to small perturbations given by the eigenvalues of the corresponding Jacobian matrix for, e.g., steady states $x^{(\mathrm{s})}$ $J_{ij} = \frac{\partial f_i}{\partial x_j}\Big|_{x=x^{(s)}}$ or the Jacobian matrix $\mathrm{J_p}$ of the Poincaré map for periodic states. Small perturbations are damped out by the

system due to dissipation, and the system returns to its original state. To view it in the picture of the stability landscape: the disturbance displaces the stable state visualized by the blue ball away from the valley and "rolls" back again due to the steepness of the walls of the potential V corresponding to the strength of the restoring forces. Directly on the hill, which relates to an unstable state, only a very small disturbance is needed to initiate the ball to "roll" either to one or the other side of the hill, depending on the direction of the disturbance. The unstable state (red ball) located on the hill of the stability landscape marks the basin boundary. This boundary separates the two basins of attraction, i.e., the two sets of initial conditions which all converge to one of the respective attractors. **In the special case of a two-dimensional system, the saddle steady state has two eigenvalues, one stable and one unstable, and the corresponding stable and unstable manifolds are onedimensional. This is illustrated in Fig. 1b. The stable manifolds along which trajectories move towards the saddle make up the basin boundaries.**

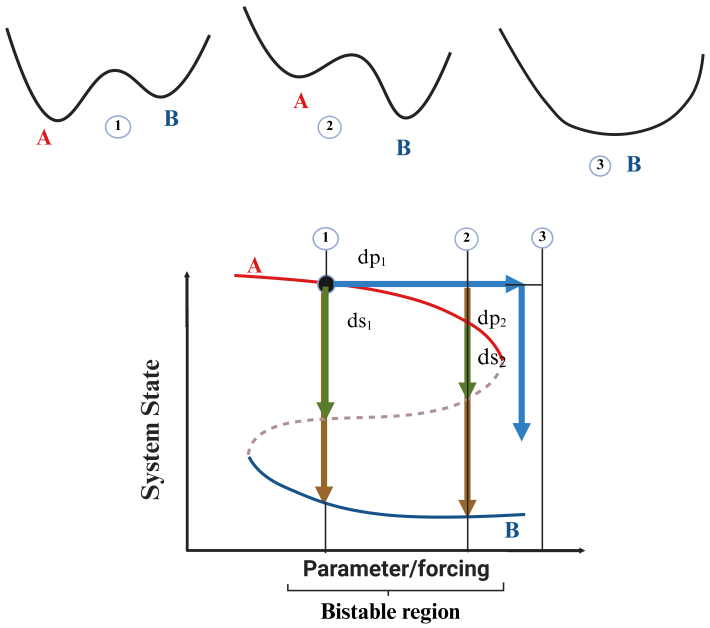

Figure 4

Often the picture of the stability landscape mentioned above is translated into a specific bifurcation diagram exhibiting hysteresis, showing the two stable states and the unstable one separating those two depending on the intrinsic parameters of the system or the external forcing, see Fig. 4. In the representation of the stability landscape, it is rather simple to explain the different disturbances that cause a system to tip. On the one hand, state variables, such as temperature and salinity, as quantities determining the water density in the ocean or the abundance of species in an ecological system can be disturbed. These disturbances correspond to the displacement of the state from the valley of the fixed stability landscape, depicted as a vertical path of perturbations $\mathrm{d}s_i$ in Fig. 4. On the other hand, disturbances in the system parameters or

external forcings change the stability landscape, corresponding to a horizontal path of perturbations $\mathrm{d}p_i$ in Fig. 4. Such disturbances can occur in three different ways: (1) fluctuations, i.e., small random perturbations of the state variables or the driving forces of the system that satisfy certain statistics; (2) large individual disturbances that correspond to extreme events or shocks; and (3) changes in environmental conditions or driving forces associated with certain trends, whereby a rate of change can characterize this trend. In nature, one would always observe a combination of these disturbances, but for theoretical investigations of tipping mechanisms, it is helpful to analyze the individual types of disturbances separately.

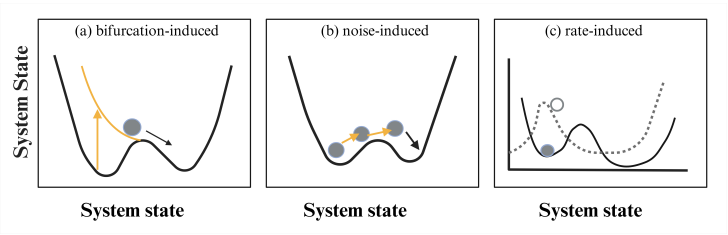

Figure 5

Next, we illustrate the different tipping mechanisms in Fig. 5, essentially following the classification introduced by Ashwin et al. Please see, Ashwin P, Wieczorek S, Vitolo R, et al. Tipping points in open systems: bifurcation, noise-induced and rate-dependent examples in the climate system[J]. Philosophical Transactions of the Royal Society A: Mathematical, Physical and Engineering Sciences, 2012, 370: 1166-1184.

Bifurcation-induced and noise-induced tipping have already been discussed in the three-box model presented in Physica D. However, the authors did not consider rate-induced tipping, which is exactly the aspect I intend to explore in my own work. Rate-induced tipping mechanism describes a system's response to an environmental change associated with a particular trend. It differs from those discussed so far by three essential points: (1) in this mechanism, the relationship between the timescales of the physical, chemical and/or biological processes in the system under consideration, i.e., the intrinsic timescales and timescale or rate of the trend of environmental changes, plays a decisive role. (2) This mechanism does not necessarily require the existence of alternative stable states. (3) The critical threshold value is not determined by a specific environmental parameter itself but by the rate of its change, which is, of course, strictly speaking, also a parameter of the system but a very particular one. In other words, the speed at which environmental changes occur is crucial. Additionally, it is important to note that this tipping phenomenon is associated with the dynamics in a non-autonomous system.

3. A simple and interesting example

In this section, we consider a unidirectionally coupled multistable system, where one subsystem (the driver) influences the other (the response), but not vice versa. This configuration is

also referred to as a drive-response or master-slave system. The system equations are:

$$\dot{X}_1 = -\left(X_1 - s_1\right)\left(X_1 - s_2\right)\left(X_1 - s_3\right) + cX_2,$$
$$\dot{X}_2 = -\varepsilon\left(X_2 - s_1\right)\left(X_2 - s_2\right)\left(X_2 - s_3\right),$$

where X_1 denotes the state of the response system, and X_2 denotes the state of the driver system. The parameters $s_1 < s_2 < s_3$ represent the locations of the fixed points in the underlying bistable dynamics of each uncoupled subsystem. The parameter c specifies the coupling strength, quantifying how strongly the driver influences the response. The parameter ε is the timescale ratio between the driver and the response subsystems, determining how fast the driver evolves relative to the response.

This coupled system is based on a canonical multistable model of the form:

$$\dot{X} = -\varepsilon\left(X - s_1\right)\left(X - s_2\right)\left(X - s_3\right),$$

which admits three steady states: two stable equilibria located at s_1 and s_3, and one unstable saddle located at s_2. To simplify the analysis, we rescale time with respect to the intrinsic timescale of the response system. This leads to a dimensionless formulation of the system, where the effective parameters are the timescale ratio $\varepsilon = \varepsilon_2/\varepsilon_1$ and the normalized coupling strength $c = C/\varepsilon_1$.

To analyze the steady-state structure of this coupled system, we examine its nullclines, defined by the conditions $\dot{X}_1 = 0$ and $\dot{X}_2 = 0$. For the driver subsystem X_2, the nullclines are horizontal lines at $X_2 = s_1, s_2, s_3$, since its evolution is independent of X_1. For the response subsystem X_1, the nullcline is given implicitly by:

$$X_2 = \frac{\left(X_1 - s_1\right)\left(X_1 - s_2\right)\left(X_1 - s_3\right)}{c}$$

which is a cubic curve in the (X_1, X_2)-plane whose shape depends on the coupling strength c. The intersections of the nullclines of X_1 and X_2 determine the equilibrium points of the full system. Depending on the parameter values c and ε, the system can exhibit two, three, or four fixed points, each corresponding to a possible long-term behavior of the coupled system.

To understand the long-term behavior of the drive-response system when the coupling strength remains fixed, we consider the so-called frozen-in case. In this setting, the parameter c, which controls the influence of the driver on the response, does not vary with time. We analyze the system by numerically simulating the evolution of trajectories from a wide range of initial conditions in the (X_1, X_2) plane. Each trajectory is integrated forward in time until it reaches a steady state, and we record which attractor it converges to. Based on this information, the state space is colored according to the attractor each initial condition ultimately reaches. The basin boundaries that emerge in this frozen-in case are invariant sets. Once a trajectory lies within one of these basins, it cannot cross into another, meaning these boundaries act as rigid separatrices in the state space.

The number and location of attractors, as well as the structure of their basins, depend strongly on the coupling strength. At higher values of c, such as 0.4 , the system typically exhibits only two stable equilibria. As c decreases, the system undergoes two saddle-node bifurcations, successively giving rise to additional pairs of attractors and saddles. At lower coupling values such as 0.1 , the system can have up to four stable equilibria, each with its own distinct basin of attraction, see Fig 6. Throughout this analysis, the parameters defining the uncoupled bistable system are fixed at $s_1 = 1.0, s_2 = 2.0$, and $s_3 = 3.0$. Only the coupling strength and the timescale ratio between the driver and the response systems are varied, allowing a focused investigation of how timescales and coupling influence multistability and basin geometry.

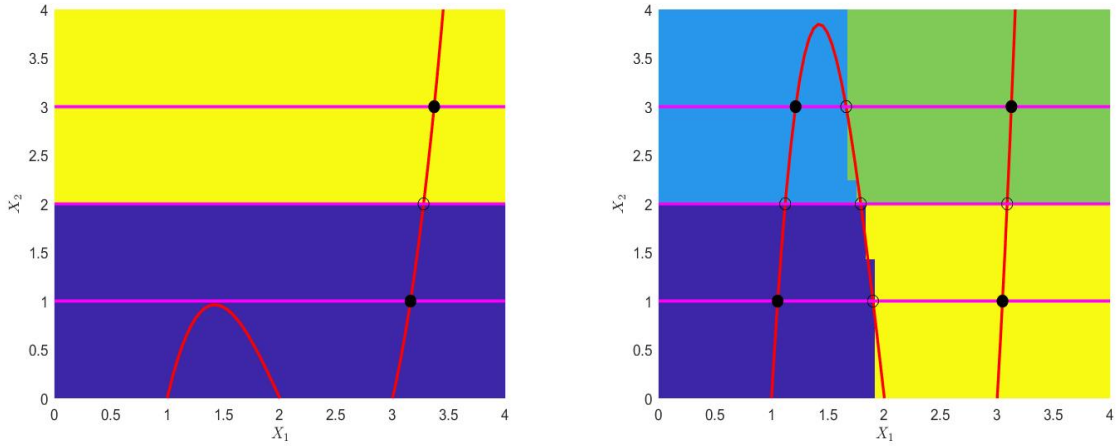

(a) (b)

Figure 6: Basins of attraction, attractors and nullclines for the autonomous system shown with fixed coupling for two different constant coupling strengths c (frozen-in case) and no timescale separation between system 1 and $2(\varepsilon = 1)$: (a) $c = 0.4$ and (b) $c = 0.1$. Attractors are indicated by a filled black circle.

To explore how a gradually changing environment influences the dynamics, we consider a nonautonomous extension of the coupled drive-response system. In this setting, the coupling strength c becomes a time-dependent parameter, decreasing linearly from an initial value $c = 0.4$ to a final value $c = 0.1$ over a finite interval. After the ramping interval, the coupling is held constant. This scenario models a common ecological or physical situation in which the external forcing evolves gradually in time. The full non-autonomous system is given by:

$$\begin{aligned}
\dot{X}_1 &= -\left(X_1 - s_1\right)\left(X_1 - s_2\right)\left(X_1 - s_3\right) + c(t)X_2, \\
\dot{X}_2 &= -\varepsilon\left(X_2 - s_1\right)\left(X_2 - s_2\right)\left(X_2 - s_3\right), \\
\dot{c} &= \begin{cases} v, & 0 \le t \le T_r, \\ 0, & T_r < t \le T_{\text{end}}, \end{cases}
\end{aligned}$$

where $c(t)$ is the time-varying coupling strength, $v = \left(c_{\text{end}} - c_{\text{start}}\right)/T_r$ is the rate of coupling change. This formulation allows us to study how the rate v of environmental change affects

the basin boundaries and tipping behavior. For instance, a slow rate may allow the system to track its moving attractors, while a fast rate can lead to abrupt transitions due to the failure of tracking. Now, we consider two different drift rates: Fast drift: $v = -0.15, T_r = 2.0$, total change $\Delta c = (c_{\text{end}} - c_{\text{start}}) = -0.3$, Slow drift: $v = -0.0375, T_r = 8.0$, same $\Delta c = -0.3$.

After T_r, the coupling remains fixed at $c = 0.1$, and the simulation continues until $T_{\text{end}} = 200$ to allow trajectories to approach their final steady states.

Two saddle-node bifurcations occur during the parameter drift. These bifurcations correspond to the appearance and disappearance of steady states due to the deformation of the response system's nullcline: The first bifurcation occurs at $c_{\text{crit 1}} = 0.3849$, corresponding to time $T_{\text{sn1}} = 0.1007$, The second bifurcation at $c_{\text{crit 2}} = 0.1283$, corresponding to $T_{\text{sn2}} = 1.8113$,

These values are analytically calculated by solving where the nullcline of X_1,

$$X_2 = \frac{(X_1 - s_1)(X_1 - s_2)(X_1 - s_3)}{c}$$

becomes tangent to the constant driver nullclines $X_2 = s_1$ or $X_2 = s_3$.

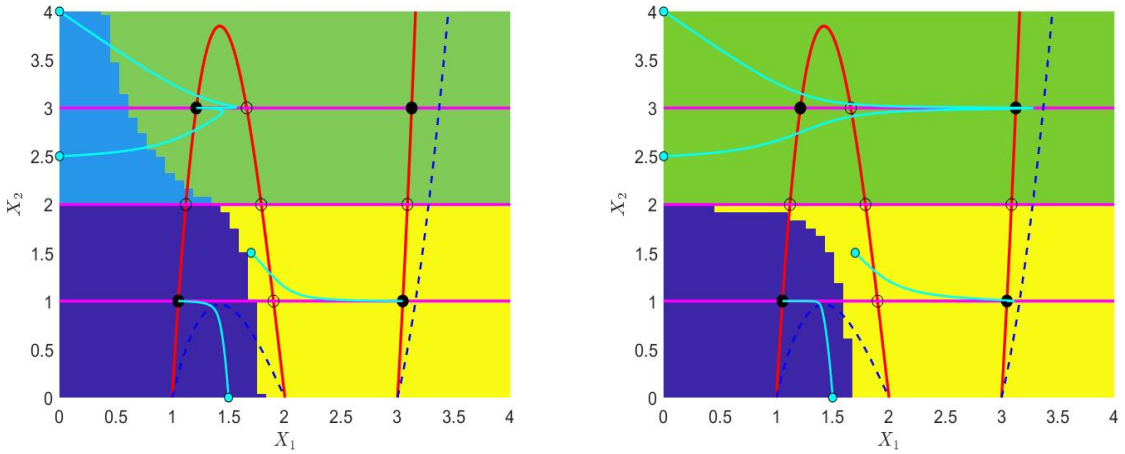

(a) (b)

Figure 7: Time evolution of the non-autonomous system with decreasing impact of the driver c in the interval $[0.4, 0.1]$ together with four exemplary trajectories ($\varepsilon = 1$) : (a) fast rate with $0 \leq t \leq 2.0, v = -0.15$ and $T_{\text{r}} = 2.0$ and (b) slow rate with $0 \leq t \leq 8.0$, $v = -0.0375$ and $T_{\text{r}} = 8.0$. Attractors are indicated by filled black circles. Dark-blue dotted curves: nullclines at the beginning of the parameter drift at $t = 0$ and $c = 0.4$; red curves: nullclines at the end of the parameter drift at $t = T_{\text{end}} = 200$ and $c = 0.1$. The non-autonomous basins of attraction are presented at the end of the simulation T_{end} in light green, yellow, violet and light blue.

To understand the global impact of the parameter drift, a grid of initial conditions is used to compute the non-autonomous basins of attraction, $\tilde{\mathcal{B}}$, defined as the set of initial states whose trajectories converge to a quasi-stationary attractor under the time-dependent dynamics. At the end of the simulation, these basins are visualized using four distinct colors, one for each stable attractor that emerges throughout the drift. To illustrate individual tipping events, four

representative initial conditions are selected. The evolution of their trajectories highlights how certain states switch basins after a bifurcation, while others remain within their original basin. Whether a trajectory tips depends on the relation between its convergence speed (dissipative timescale) and the drift speed of $c(t)$. When the environmental change is slow, trajectories can "track" the evolving attractors. When the change is fast, the system cannot adapt quickly, and trajectories may enter a different basin, leading to tipping, see Fig 7.

It is worth noting that this simple multistable system exhibits a phase plane structure that closely resembles that of the three-box model. From a dynamical perspective, this suggests that similar rate-induced tipping phenomena are also likely to occur in the three-box model.

4. Reflections and open questions

1. Do you think it is worthwhile to investigate rate-induced tipping in the three-box model?

To better represent gradual changes in external climatic forcing, we extend the model by allowing the freshwater forcing parameter F to vary explicitly with time. In particular, we consider a linear drift of the form $F(t) = F_0 + rt$, where F_0 is the initial freshwater forcing and r denotes the drift rate. This transforms the original model into a non-autonomous system capable of capturing rate-induced tipping phenomena.

The full system of equations becomes:

$$\begin{aligned}
V_L \frac{dS_L}{dt} &= -\left(F(t) + F_N + \eta\left(F_L - F_N\right)\right) S_0 + |q_L|\left(S_A - S_L\right), \\
V_N \frac{dS_N}{dt} &= -\left(F(t) + F_N\right) S_0 + |q_N|\left(S_A - S_N\right), \\
V_{\text{Total}}\, S_0 &= V_L S_L + V_A S_A + V_N S_N, \\
q_L &= -k\left[\alpha\left(T_N + \mu\left(T_L - T_N\right) - T_A\right) - \beta\left(S_L - S_A\right)\right], \\
q_N &= -k\left[\alpha\left(T_N - T_A\right) - \beta\left(S_N - S_A\right)\right].
\end{aligned}$$

Introducing an explicit time-dependence in the freshwater forcing parameter $F(t) = F_0 + rt$ is motivated by real-world climate processes, where freshwater input into the North Atlantic does not change abruptly but accumulates gradually over time. This includes, for example, the progressive melting of the Greenland ice sheet, increased Arctic river discharge, or long-term shifts in precipitation patterns. Such processes unfold over decades to centuries, and their impact on the AMOC depends not only on the total amount of freshwater added, but also on the rate at which this addition occurs.

By treating F as a slowly drifting variable, the model becomes non-autonomous, which enables the study of rate-induced tipping. This mechanism captures situations where the AMOC can abruptly collapse even if the final forcing level alone would not be sufficient to destabilize it under equilibrium conditions. In other words, it highlights the fact that the pace of change itself can be destabilizing. Such insights are essential for assessing the near-term risks of AMOC

weakening under plausible future climate trajectories and are not accessible through traditional bifurcation or stochastic noise analysis alone.

2. In the region highlighted by the pink ellipse, the system undergoes a non-smooth saddle-node bifurcation. I was wondering whether this type of bifurcation leads to any distinct dynamical features compared to the classical smooth case. From numerical simulations, they both seem to result in a similar hysteresis structure.

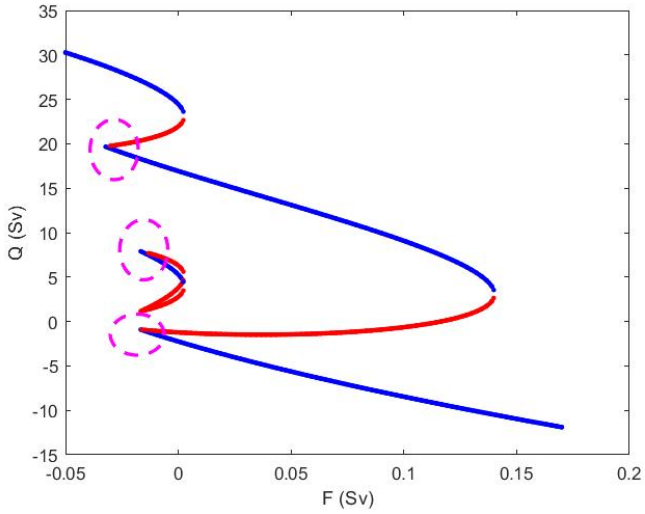

Figure 8

3. The three-box model includes absolute value terms, which introduce non-smoothness into the system. I'm not very familiar with how such non-smooth features might affect the dynamics. Do you think it would be worthwhile to explore whether this non-smoothness leads to any special phenomena? If possible, perhaps you could consider some preliminary work on this aspect, and we could then discuss it further together.

4. To be honest, my strength lies more in numerical work rather than theoretical derivations. I'm more comfortable using computational tools to explore dynamical behaviors. Perhaps we could have a discussion about where to place the emphasis in the next stage of work? I'd also be very interested to hear your thoughts on what kinds of models or specific problems might be worthwhile to explore further.

References

[1] P. Ashwin, S. Wieczorek, R. Vitolo, and P. Cox. Tipping points in open systems: bifurcation, noise-induced and rate-dependent examples in the climate system. *Philosophical Transactions of the Royal Society A: Mathematical, Physical and Engineering Sciences,* **370** (2012) 1166–1184.

[2] A. Neff, A. Keane, H. A. Dijkstra, and R. V. Donner. Bifurcation analysis of a North Atlantic Ocean box model with two deep-water formation sites. *Physica D: Nonlinear Phenomena,* **456** (2023) 133907.

[3] P. Ashwin, C. Perryman, and S. Wieczorek. Parameter shifts for nonautonomous systems in low dimension: bifurcation- and rate-induced tipping. *Nonlinearity,* **30** (2017) 2185–2210.

[4] B. Kaszás, U. Feudel, and T. Tél. Tipping phenomena in typical dynamical systems subjected to parameter drift. *Scientific Reports,* **9** (2019) 8654.

[5] C. Budd and R. Kuske. Dynamic tipping and cyclic folds in a one-dimensional non-smooth dynamical system linked to climate models. *Physica D: Nonlinear Phenomena,* **457** (2024) 133949.